

Thermodynamics and Kinetics of NaAlH₄ Nanocluster Decomposition

Supporting Information

Raghunandan K. Bhakta,¹ Sean Maharrey,² Vitalie Stavila,² Aaron Highley,² Todd Alam,³ Eric Majzoub,⁴ and Mark Allendorf^{1}*

¹ Energy Nanomaterials Dept., Sandia National Laboratories, Livermore, CA 94551-0969

² Combustion Research Facility, Sandia National Laboratories, Livermore, CA 94551-0969

³ Sandia National Laboratories, Albuquerque, NM 87185

⁴ Dept. of Physics, University of Missouri, St. Louis, MO 63130

mdallen@sandia.gov

STMBMS (Simultaneous Thermogravimetric Modulated Beam Mass Spectrometry)

This instrument allows the concentration and release rate of each gas-phase species in a reaction cell (Fig. S1) to be measured as a function of time by correlating the ion signals at different m/z values measured with a mass spectrometer with the rate of force change measured by a micro balance at any instant. A small sample of material (~ 10 mg) is placed in an alumina reaction cell that was then mounted on a thermocouple probe, which was seated on a microbalance. The reaction cell was enclosed in a high vacuum environment ($<10^{-6}$ Torr) and was radiatively heated by a bifilar-wound tungsten wire on an alumina tube. The molecules from the gaseous mixture in the reaction cell exit through an orifice in the cap of the reaction cell and traverse two beam-defining orifices before entering the electron-bombardment ionizer of the mass spectrometer where the ions were created by collisions of 20-eV electrons with the different molecules in the gas flow. The background pressure in the vacuum chamber housing the reaction cell is sufficiently low to eliminate significant scattering between molecules evolving from the reaction cell and background molecules prior to entering the MBMS detection system. The different m/z value ions were selected with a quadrupole mass filter and counted with an ion counter. The gas flow was modulated with a chopping wheel and only the modulated ion signal was recorded.

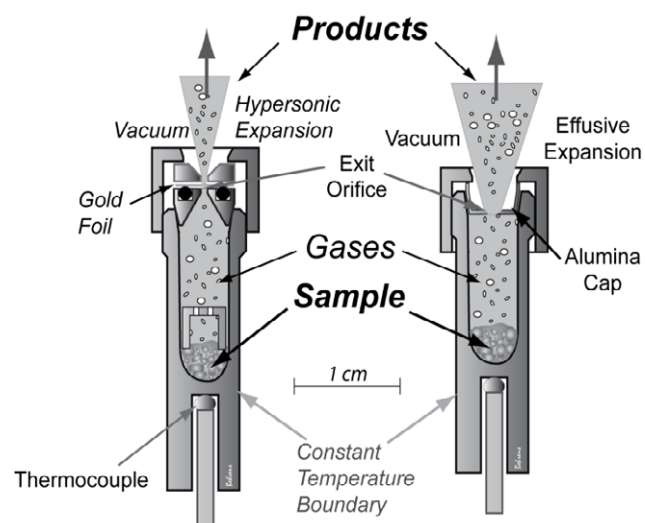


Figure S1. Cross section of reaction cells used in STMBMS experiments.

The reaction conditions within the cell are controlled and varied by adjusting the rate at which gas exits the reaction cell. The rate of flow of gas from the cell, and the corresponding containment time of gas within the cell, are a function of the orifice area, the free volume within the reaction cell, and the characteristics of the flow of gas through the orifice. Orifices spanning a broad range of diameters (1000 to $2.5\mu\text{m}$) can be used in experiments to span a broad range of the confined gas parameter space. This allows the partial pressures of the gases contained within the reaction cell to be varied between 10^{-5} and 1000 Torr. Orifices with diameters ranging from 1000 to $35\mu\text{m}$ in diameter use an alumina cap and orifices with the $25\mu\text{m}$ and smaller use the gold foil/rubber o-ring seal (Fig S1). For these experiments, 1000 and $400\mu\text{m}$ orifices were used for evaporative drying of solvents, while 25 and $10\mu\text{m}$ orifices were used for probing the kinetics of the hydrogen release process.

In a typical experiment, the sample is loaded into the reaction cell within an inert atmosphere glove box, fitted with the cap and then transported under an inert atmosphere and placed in the STMBMS instrument. The STMBMS instrument is then evacuated and data acquisition commences

approximately one hour later. The samples are either heated at a low isothermal temperature (110°C) to evolve solvents, or a series of isothermal steps spanning above and below the melting point are used. The data have been quantified using the ion signal representing the main species that accounts for the mass loss: H₂.

Additional sample characterization data

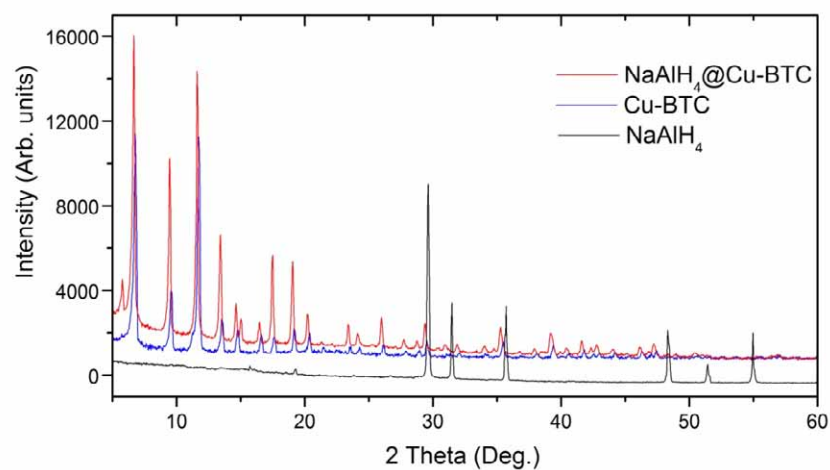


Figure S2. X-ray diffraction of Cu-BTC MOF in comparison with infiltrated material $\text{NaAlH}_4@\text{Cu-BTC}$ and pure NaAlH_4 .

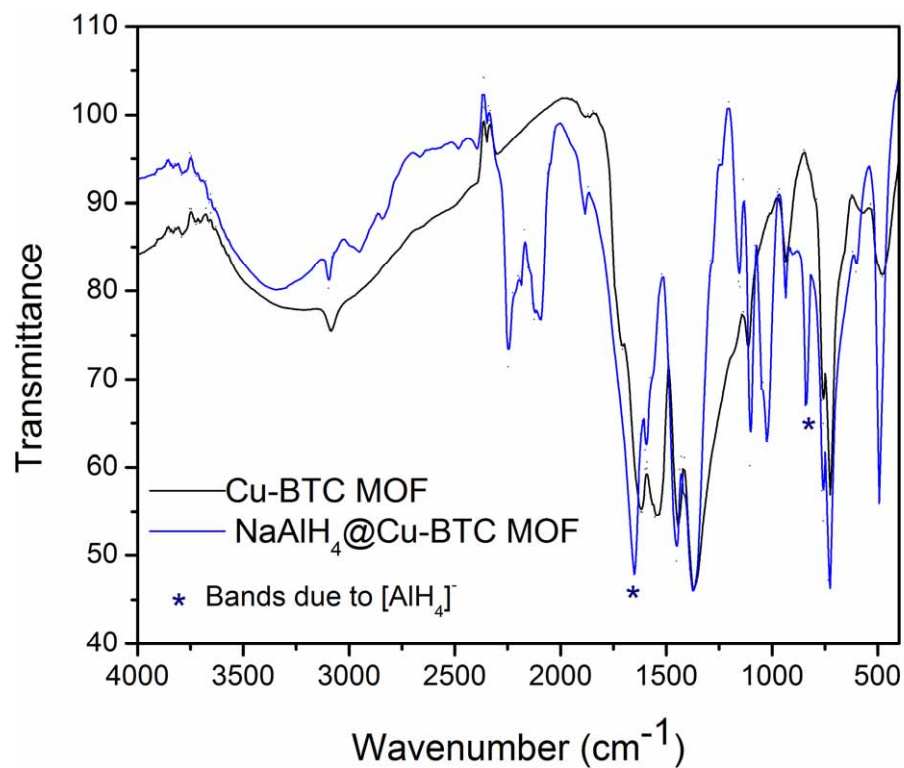


Figure S3. FTIR spectrum of neat Cu-BTC MOF (Black) and $\text{NaAlH}_4@\text{Cu-BTC MOF}$ (Blue), * indicate the bands assigned to $[\text{AlH}_4]^-$.

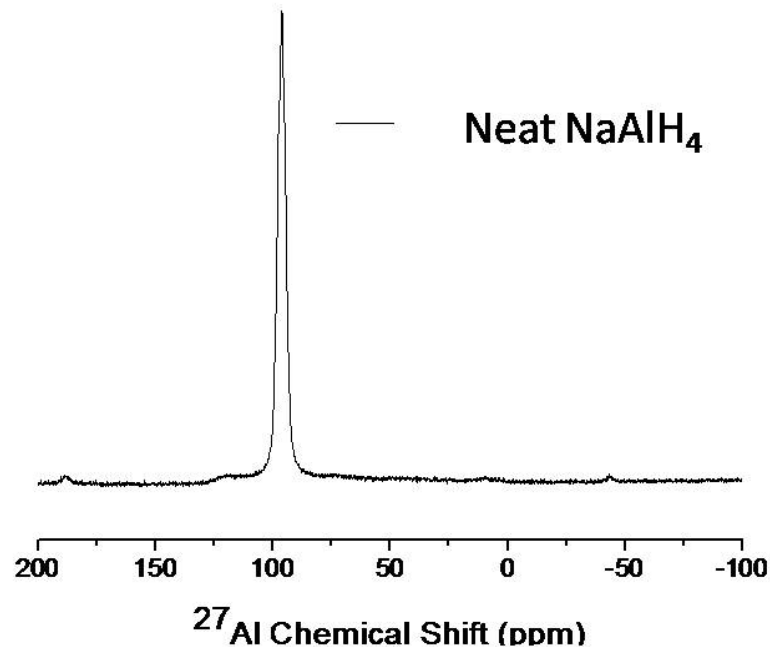


Figure S4. ^{27}Al MAS NMR spectra of neat NaAlH_4 .

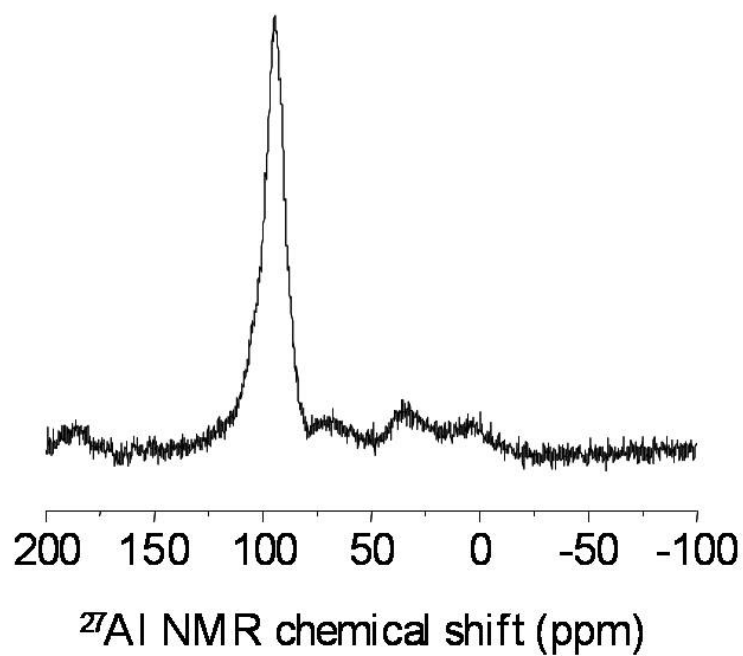


Figure S5. The ^{27}Al MAS NMR of of NaAlH_4 @Cu-BTC, NaAlH_4 has a chemical shift of 94.6ppm. Some Al_2O_3 impurity peaks are also observed at 8.4, 35.5 and 63.6 ppm respectively.

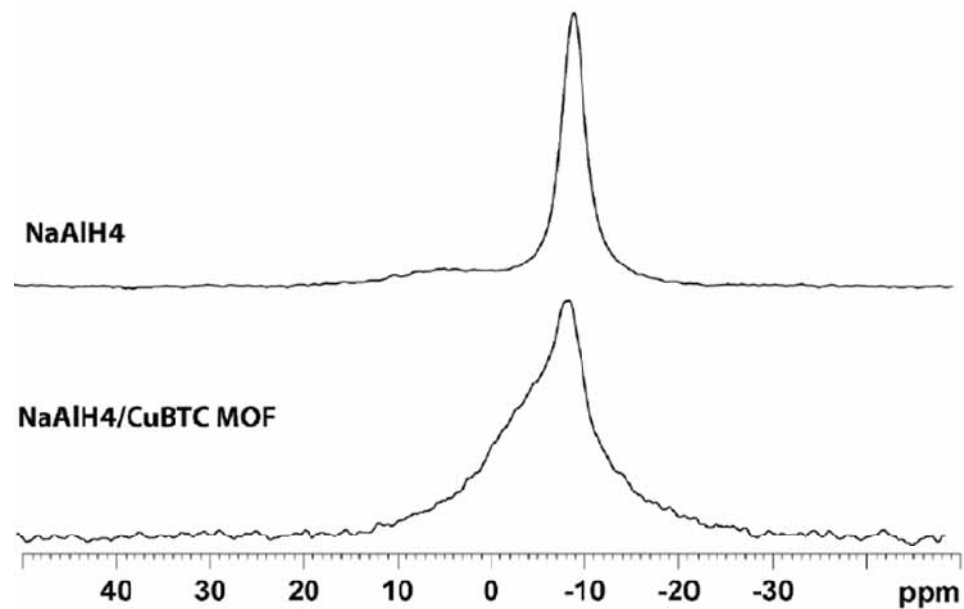


Figure S6. ^{23}Na MAS NMR spectra of neat NaAlH₄ and NaAlH₄@Cu-BTC.

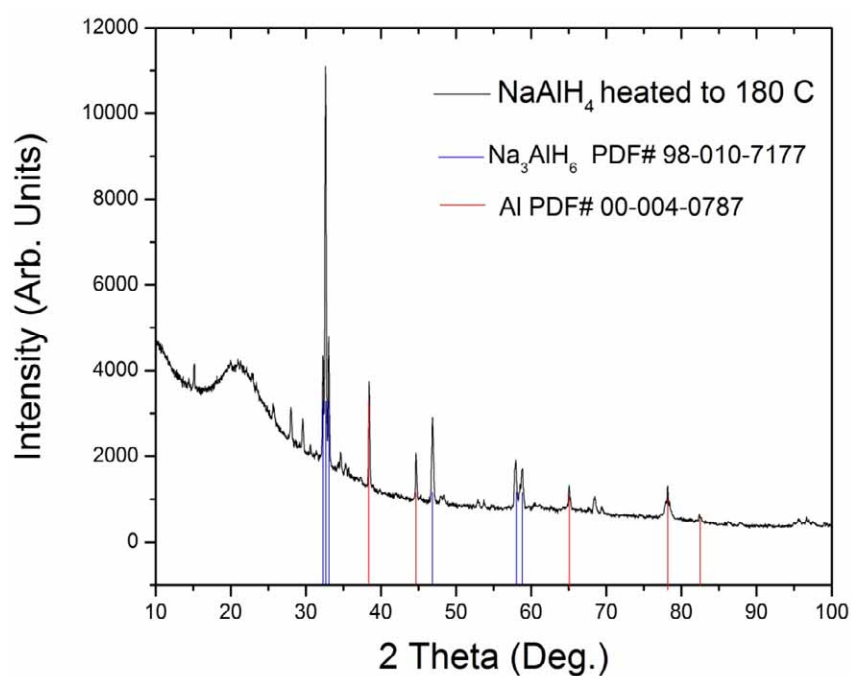


Figure S7. Powder XRD analyses of NaAlH₄ heated at 180 °C indicating reflections due to Al and Na₃AlH₆.

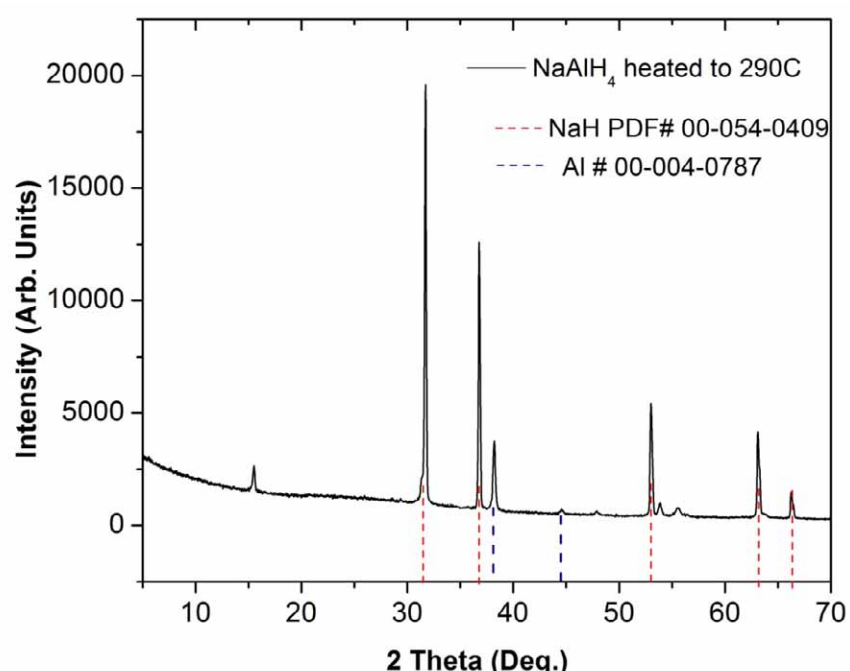


Figure S8. Powder XRD analyses of NaAlH₄ heated at 290 °C indicating reflections due to Al and NaH.

Bulk NaAlH₄ hydrogen desorption thermodynamics and kinetics

The thermodynamic and kinetic behavior of bulk NaAlH₄ is discussed here, so that the substantial differences between this material and NaAlH₄@Cu-BTC are apparent. As indicated in Figure S-9A, the decomposition reaction was observed over the course of a two-segment temperature program in which the temperature was increased in 10 °C steps, first to maximum of 210 °C, followed by a second segment to 315 °C. Separate experiments were run with 5°C isothermal steps in the first thermal segment to capture additional details of intermediate steps involved in reaction (1). These data were used for the corresponding quasi-equilibrium and kinetic analyses shown in Figures 3 and 4, respectively.

We observe two distinct decomposition steps, illustrated by the weight loss data shown in Sup. Info. Figure S-9A and the corresponding evolution of H₂ in Sup. Info. Figs. S-9C and S-9D. Based on the computed sample stoichiometry as a function of time, these steps can be correlated with the global reactions (1) and (2). In the following discussion, we will refer to the multi-step mechanisms underlying reactions (1) and (2) as decomposition process 1 (DP-1) and decomposition process 2 (DP-2), so that we can differentiate between the detailed kinetic processes and the global reactions. DP-1 encompasses all of the first thermal segment and up to ~230 °C in the second segment. During the cooling portion of segment 1 (plateau between ~ 40,000 – 70,000 s), DP-1 is effectively ‘quenched,’ then resumes when the temperature reaches 210°C during the heating portion of segment 2. DP-1 is complete during the 230°C isotherm (81000-85000 s). The hydrogen stoichiometry at this point is ~2.1, which is consistent with the change expected from reaction (1) and results in formation of Na₃AlH₆, as seen in the PXRD pattern (Sup. figure S-7).

The onset of DP-2 occurs during the 260 °C isotherm of the second heating segment (95000-99000 s in Sup. Figure S-9) and continues to the maximum temperature of the experiment (315 °C). This process produces a net loss of 25% of the initial hydrogen, resulting in an overall reduction in the condensed-phase hydrogen stoichiometry from 2.1 to 1.19. This is again consistent with the known second step in NaAlH₄ decomposition (reaction (2)), leading to formation of NaH (see PXRD in figure S-8). The final

hydrogen stoichiometry of ~1.19 suggests that a small amount of Na_3AlH_6 remains unreacted at the end of the experiment, which was limited to 320°C because of the Kalrez o-rings used to seal the reaction cell.

The rate of H_2 release throughout the course of the experiment, shown in Figure Sup. Figure S-9B – 9D, illustrates the complex temperature-dependent kinetic behavior that this hydride undergoes. It appears that during DP-1 at least four different chemical events are occurring (Sup. Figure S-9C). Three of these are kinetically limited (indicated by a time-dependent H_2 GER during the isothermal step), while the fourth is at quasi-equilibrium (constant GER during the isothermal step). Although we lack the detailed phase and microstructural information required to definitively assign a mechanism to each of these, the shape of the H_2 GER curve at each isothermal step provides a qualitative indication of the type of reaction process occurring at that temperature. Initially, the H_2 release resembles a nucleation and growth process (see kinetic analysis below). At $< 165^\circ\text{C}$ ($0 - 17000$ s), only 0.35 equivalents H_2 are lost from the sample. A second process begins at $\sim 170^\circ\text{C}$ ($17500 - 19000$ s); here, the time-dependent GER is indicative of solid-solid phase-transitions (based on previous systems investigated by STMBMS). This is followed by a third process ($20500 - 22500$ s) that is consistent with incongruent melting at the reported NaAlH_4 melting point of 181°C .⁴⁵ In this step, virtually all of the remaining hydrogen corresponding to process (1) is released. Finally, a quasi-equilibrium process occurs at $190 - 200^\circ\text{C}$ ($26500 - 33500$ s). Note that, since the stoichiometry indicates that some NaAlH_4 remains unreacted at the conclusion of the first heating segment, this quasi-equilibrium likely involves solid and liquid-phase NaAlH_4 as well as H_2 .

In contrast, DP-2, which commences during the second heating segment at temperatures 260°C ($t \geq 95,000$ s; Sup. Figure S-9D) displays only two processes: a quasi-equilibrium at temperatures below 290°C ($95000 - 113000$ s) and a nucleation and growth stage at $300 - 310^\circ\text{C}$ ($114000 - 120000$ s). It therefore appears that, in contrast with DP-1, in which improved mass transport resulting from the formation of a liquid phase accelerates decomposition, the decomposition of these products occurs without melting. The segment (2) data display no evidence of a melting transition, nor of the known α - β phase transition that Na_3AlH_6 is known to undergo at 252°C . The latter is observed only at high heating rates ($20^\circ\text{C}/\text{minute}$),⁵² which are not achieved in our experiments.

The quasi-equilibrium behavior seen in DP-1 ($T = 190 - 210^\circ\text{C}$ in segment (1) and $T = 185 - 210^\circ\text{C}$ in segment (2); Table ST1 and ST2 can be analyzed using the van't Hoff equation to obtain the enthalpy of H_2 desorption ΔH_d° , as shown in Figure 3. The values obtained from the first and second heating segments are $37.3 \text{ kJ} \cdot (\text{mol H}_2)^{-1}$ and $35.2 \text{ kJ} \cdot (\text{mol H}_2)^{-1}$, respectively, which agree very well with the value reported for reaction (1) in the absence of a catalyst ($36.7 \text{ kJ} \cdot (\text{mol H}_2)^{-1}$).³⁵ The quasi-equilibrium behavior for DP-2 ($T = 260 - 290^\circ\text{C}$ in segment (2); Table ST1) gives a reaction enthalpy of $21.2 \text{ kJ} \cdot (\text{mol H}_2)^{-1}$ for reaction (2) (Figure S10), which also is in good agreement with the literature value of $23.2 \text{ kJ} \cdot (\text{mol H}_2)^{-1}$.³⁵

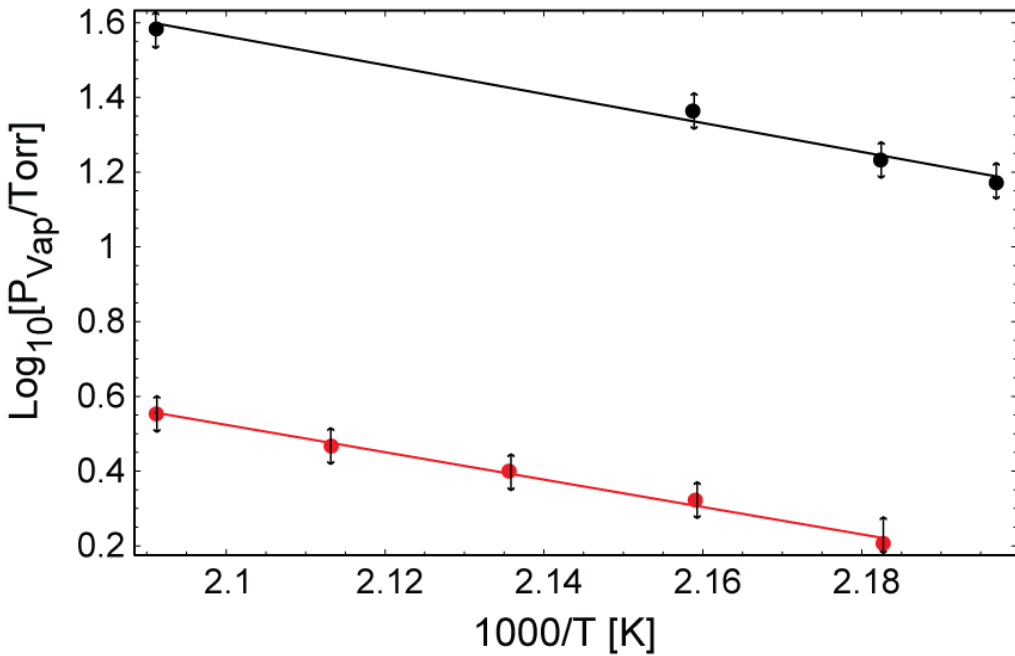


Figure S9A. Reaction enthalpies for the equilibrium-like hydrogen release sequence for Bulk NaAlH₄.

- Data from first heating segment $\Delta H_d = 37.3 \text{ kJ} \cdot (\text{mol H}_2)^{-1}$.
- Data from second heating segment below 220°C, $\Delta H_d = 35.2 \text{ kJ} \cdot (\text{mol H}_2)^{-1}$.

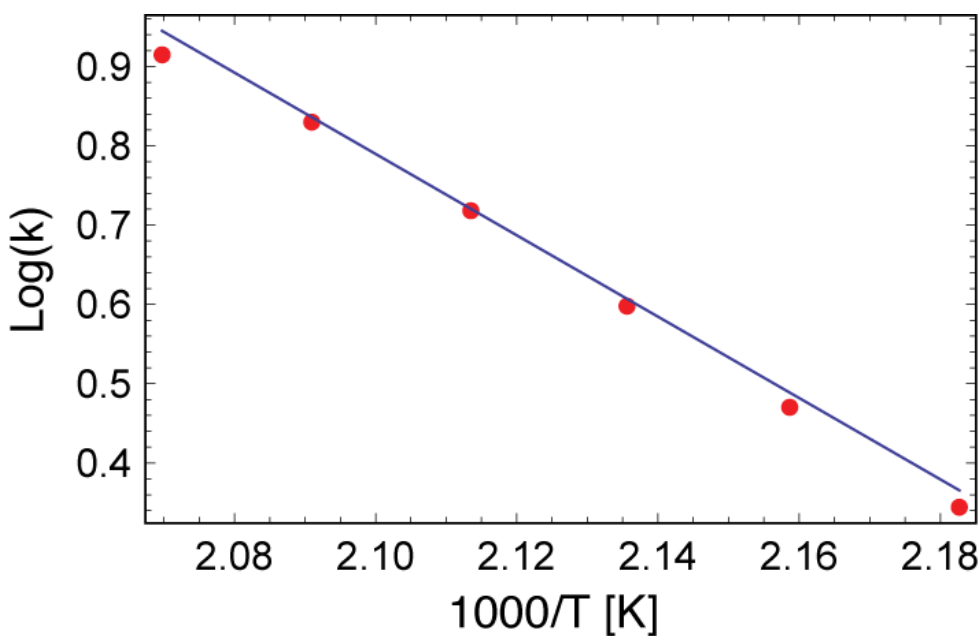


Figure S9B. Kinetic analysis of H₂ desorption for bulk NaAlH₄, nucleation and growth model fit. $E_a = 98.2 \text{ kJ} \cdot (\text{mol H}_2)^{-1}$ (Error bars are too small to be seen).

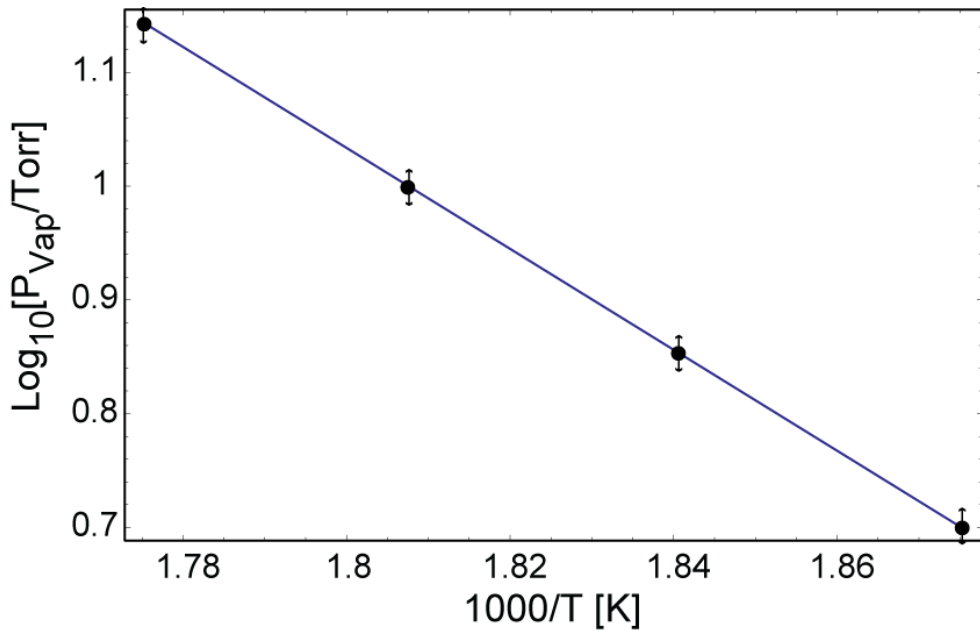


Figure S10. Reaction enthalpy for the quasi-equilibrium hydrogen release from bulk NaAlH₄. ● Data from second heating segment above 260°C $\Delta H_d = 21.2 \text{ kJ} \cdot (\text{mol H}_2)^{-1}$.

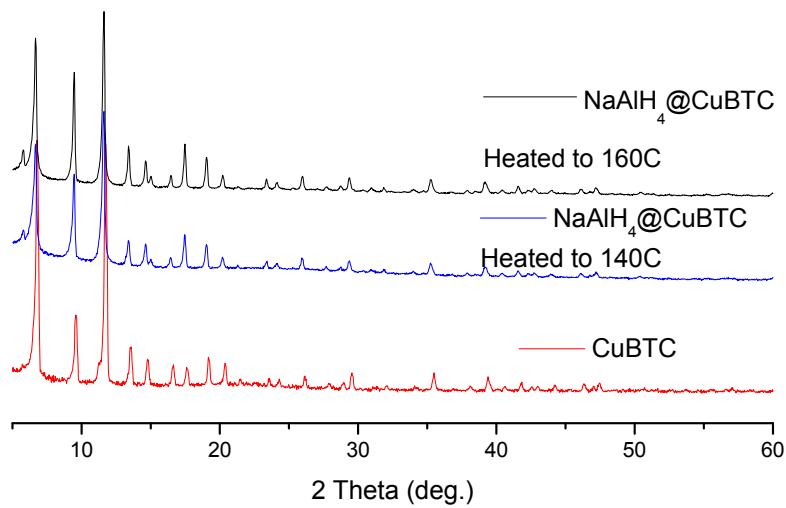


Figure S11. Powder XRD analyses of reaction intermediates of NaAlH₄@Cu-BTC heated at 140 and 160 °C do not indicate any reflections due to NaAlH₄ or Na₃AlH₆.

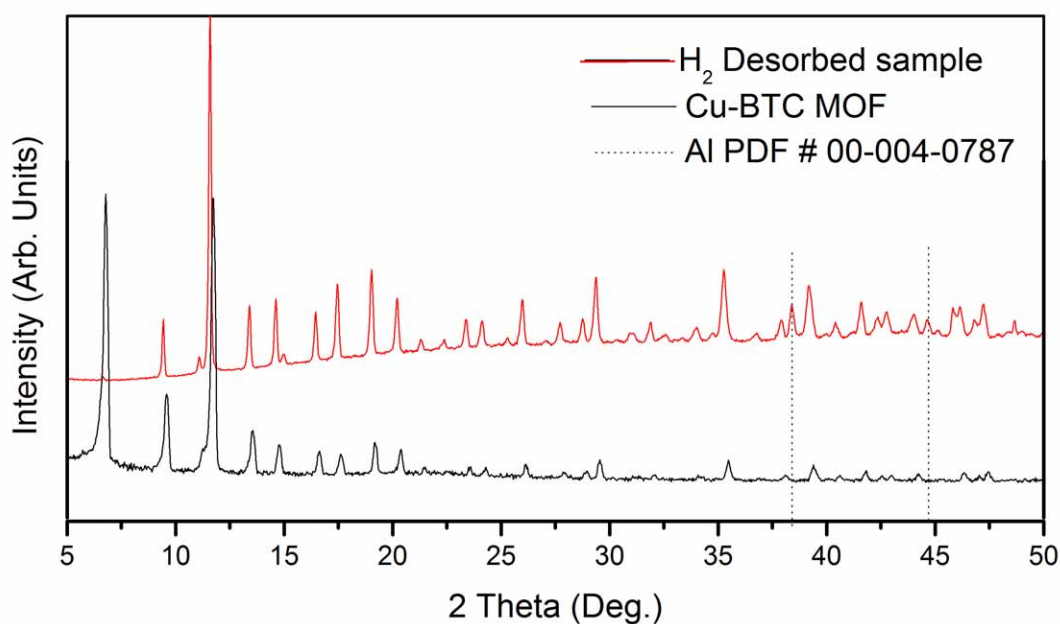


Figure S12. X-ray diffraction of Cu-BTC MOF in comparison with infiltrated material NaAlH₄@ Cu-BTC after H₂ desorption. Dotted lines indicate Aluminum reflections.

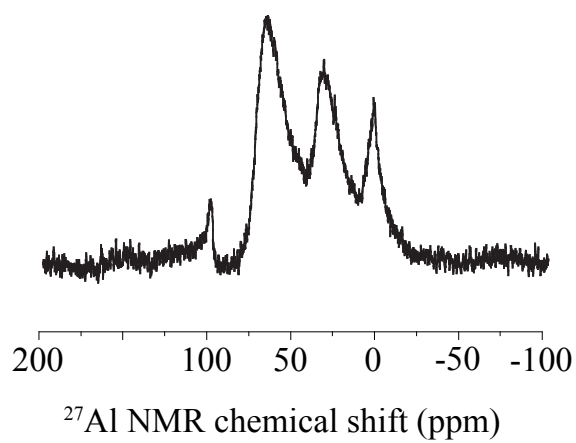


Figure S13. ²⁷Al MAS NMR of NaAlH₄@Cu₃(BTC)₂ after desorption. The three peaks at 8.4, 35.5, and 63.6 ppm are assigned to Al₂O₃, which forms when the decomposition product Al reacts with O₂ during brief exposure to the air during sample transfer.

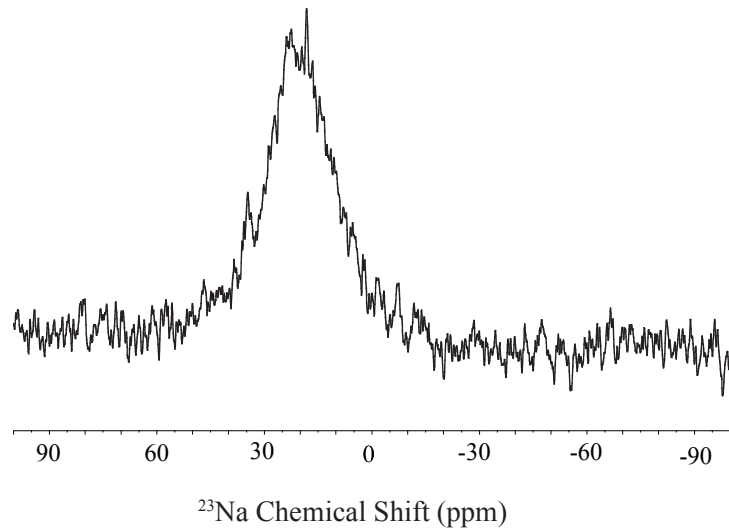


Figure S14. ^{23}Na MAS NMR of $\text{NaAlH}_4@\text{Cu}_3(\text{BTC})_2$ after H_2 desorption shows a broad peak at 19.3 ppm, which represents NaH . This was confirmed by running a ^{23}Na NMR experiment on NaH .

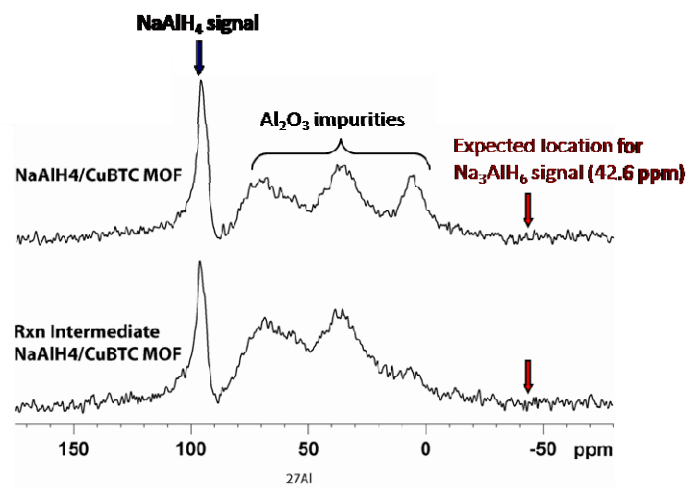


Figure S15. Solid state NMR analyses of reaction intermediates of $\text{NaAlH}_4@\text{Cu-BTC}$ heated at 135C do not indicate any signal due to Na_3AlH_6 .

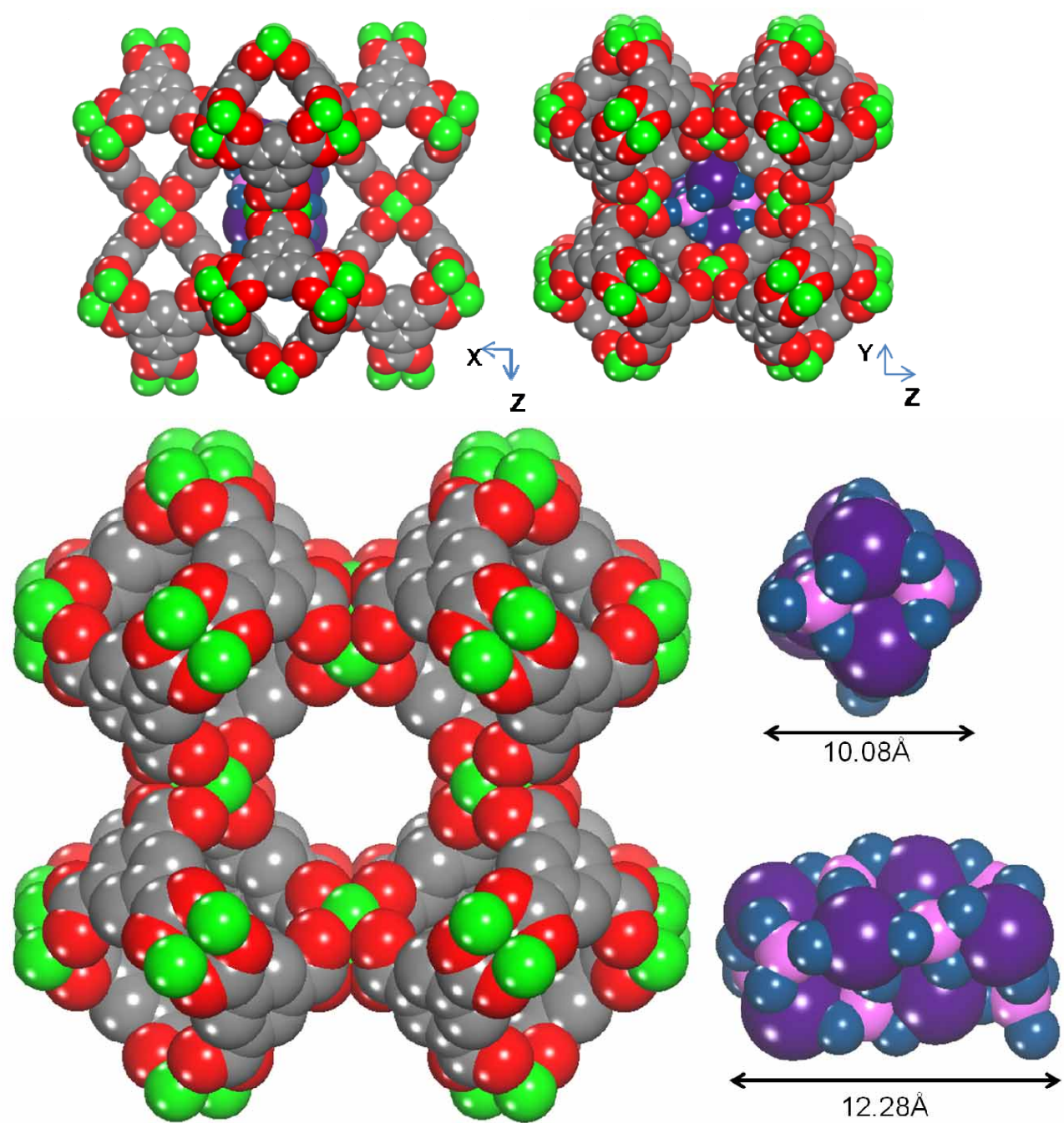


Figure S16. Schematic figure showing 8 formula units of NaAlH₄ inside the large pore of Cu-BTC MOF oriented along XZ and YZ axes.

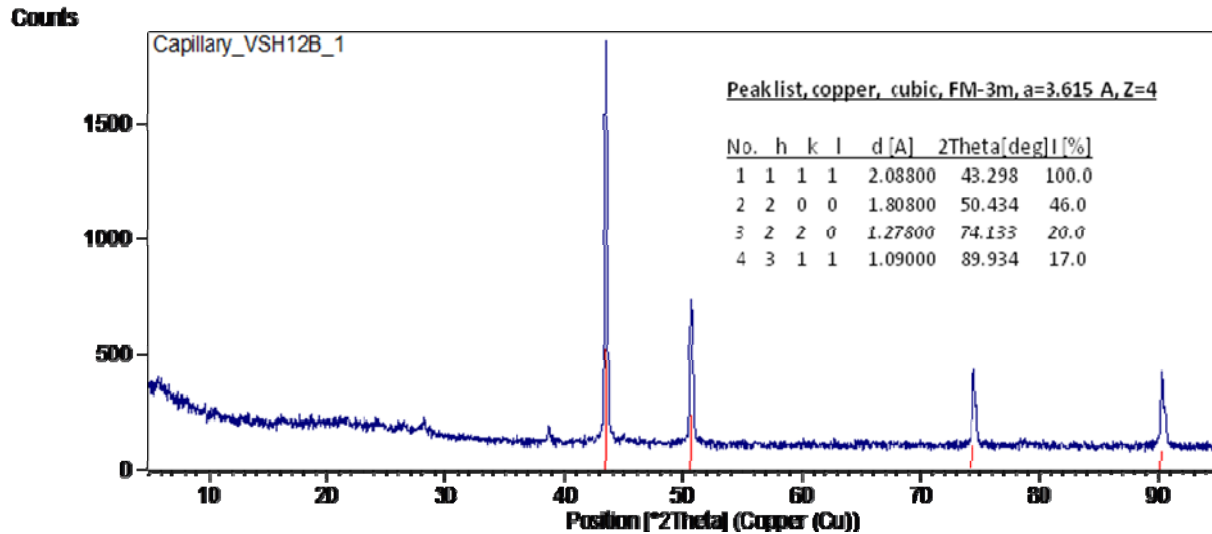
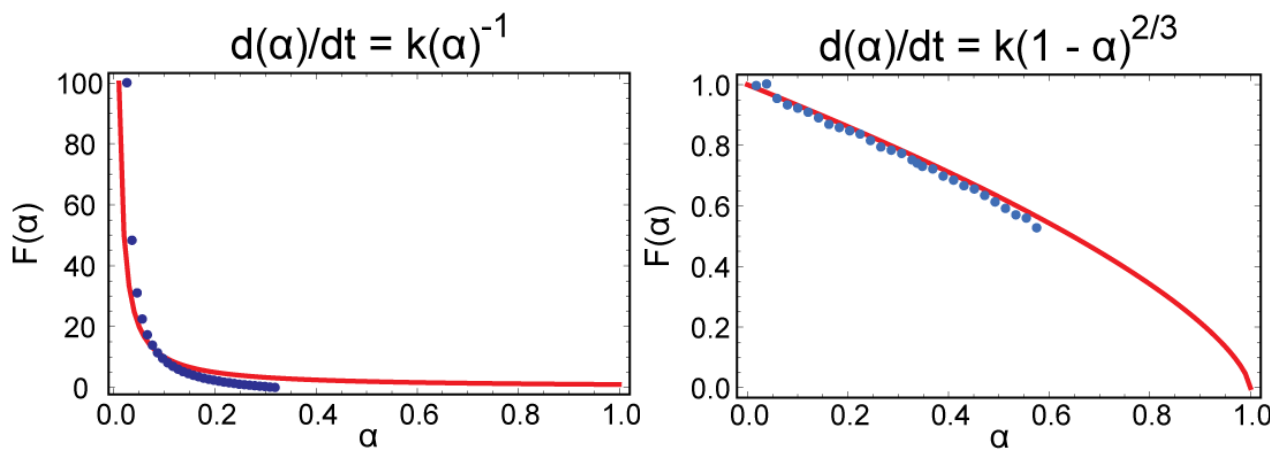


Figure S17. Powder XRD of CuBTC after attempt to rehydrogenate under 120bar H₂ and 150 °C indicating collapse of the framework, Only reflections due to copper are seen.



Sup. Figure S18. Typical examples of fits to solid-state reaction models of the STMBMS H₂ desorption data. Left: 1-D diffusion model for NaAlH₄@Cu-BTC. Right: nucleation and growth model for bulk NaAlH₄. In both plots, the solid line (red) is the model fit for the function indicated above the plot. Data points (blue symbols) are the quantified data corresponding to one measured rate constant at particular temperature isotherm in the data set to illustrate quality of the fit to the data. For example, the rate constant *k* extracted from plots such as those above corresponds to a single data point shown in Figure 6. To obtain the fits, the raw GER data were converted from a function of time to a function of alpha (the extent of reaction variable) using the mass loss within a given temperature step. The data were also scaled by the *k*-value for that particular temperature step so they can be superimposed on the generic model; i.e., the model is a function of $F(\alpha) = f(\alpha)$, while the data are a function $D(\alpha) = k(T)f(\alpha)$. Finally, the size of the data points is representative of ~ 50% of the error bars for each data set. Each

isotherm was fit to a total of 16 different solid-state reaction models. A cutoff for R^2 of 0.98 was used accept a given fit for further analysis. The data represented by the 1-D diffusion model and the nucleation and growth model have R^2 values higher than 0.98, while the other 15 models for each data set were rejected for further analysis as none showed a fit better than 0.88.

Table S-1. Temperature profile used for STMBMS experiment on bulk NaAlH₄.

Time (s)	Temperature (°C)	Process	Reaction Energy (kJ/Mol H ₂)		Hydrogen Stoichiometry Change
			ΔEa	ΔHd	
First heating segment					
0 - 500	25				
2000 - 7000	150				
7300 - 11300	160				
11600 - 15600	165				
15900 - 19900	170				
20200 - 24200	175				
24380 - 28380	178				
28620 - 32620	182	Quasi-Equilibrium			37.3
32800 - 36800	185				
37100 - 41100	190				
50000 - 54000	205				
54300 - 58300	210				
58600 - 62600	205				
62900 - 66900	200				
67200 - 71200	195				
71500 - 75500	190				
75800 - 79800	185				
80100 - 84100	190				
Second heating segment					
84400 - 88400	195	Quasi-Equilibrium			2.3 - 2.1
88700 - 92700	200				
93000 - 97000	205				
97300 - 101300	210				
101600 - 105600	205				
105900 - 109900	200				
110200 - 114200	195				
114500 - 118500	190				
118800 - 122800	185				
123100 - 127100	180				
127400 - 131400	175				

131700 - 135700	170				
136000 - 140000	165				

Table S-2. Temperature profile used for STMBMS experiment on bulk NaAlH₄ to get more information on quasi equilibrium process between 26-290C .

Time (s)	Temperature (°C)	Process	Reaction Energy (kJ/Mol H ₂)		Hydrogen Stoichiometry Change
			ΔE _a	ΔH _d	
First heating segment					
0 - 500	30				
1820 - 6820	140				
7420 - 11420	150				
12020 - 16020	160				
16620 - 20620	170				
21220 - 25220	180				
25820 - 29820	190				
30420 - 34420	200				
35020 - 39020	210				
39620 - 43620	200				
44220 - 48220	190				
48820 - 52820	180				
53420 - 57420	170				
Second heating segment					
58020 - 62020	180				
62620 - 66620	190				
67220 - 71220	200				
71820 - 75820	210				
76420 - 80420	220				
81020 - 85020	230				
85620 - 89620	240				
90220 - 94220	250				
94820 - 98820	260	Quasi-Equilibrium			
99420 - 103420	270				
104020 - 108020	280				
108620 - 112620	290				
113220 - 117220	300				
117820 - 121820	310				
122120 - 126120	315				
126420 - 130420	310				
131020 - 135020	300				
135620 - 139620	290				
140220 - 144220	280				
144820 - 148820	270				

149420 - 153420	260				
154020 - 158020	250				
158620 - 162620	240				
163220 - 167220	230				
167820 - 171820	220				
172420 - 176420	210				
177020 - 181020	200				
181620 - 185620	190				
186220 - 190220	180				
190820 - 194820	170				
195690	25				

Table S-3. Temperature profile used for STMBMS experiment on NaAlH₄@Cu-BTC.

Time (s)	Temperature (°C)	Process	Reaction Energy (kJ/Mol H ₂)		Hydrogen Stoichiometry Change
			ΔE _a	ΔH _d	
First heating segment					
0 - 500	25				
3050 - 8050	110	Quasi-Equilibrium			47.3
8650 - 12650	120				
13250 - 17250	130				
17550 - 21550	135	1-D Diffusion	53.3		3.75 - 2.95
21850 - 25850	140				
26150 - 30150	145				
30450 - 34450	150				
34750 - 38750	155				
39050 - 43050	160				
43350 - 47350	165				
47650 - 51650	170				
51950 - 55950	165				
56250 - 60250	160				
60550 - 64550	155				
64850 - 68850	150				
69150 - 73150	145				
73450 - 77450	140				
77750 - 81750	135				
82050 - 86050	130				
86650 - 90650	120				
91250 - 95250	110				
Second heating segment					
95850 - 99850	120				
100450 - 104450	130				
105050 - 109050	140	Quasi-Equilibrium		45.6	2.05 - 1.92
109650 - 113650	150				
114250 - 118250	160				

118550 - 122550	165				
122850 - 126850	170				
127150 - 131150	175				
131330 - 135330	178				
135570 - 139570	182				
139750 - 143750	185				
144050 - 148050	190				
148350 - 152350	195				
152650 - 156650	200				
156950 - 160950	205				
161250 - 165250	210				
165550 - 169550	205				
169850 - 173850	200				
174150 - 178150	195				
178450 - 182450	190				
182750 - 186750	185				
187170 - 191170	178				
192088	25				